 doi:10.20944/preprints202209.0329.v1

Article

Diffusion and Velocity Correlations of the Phase Transitions in a System of Macroscopic Rolling Spheres

F. Vega Reyes [1,2], A. Rodríguez-Rivas [3], J. F. González-Saavedra [1] and M. A. López-Castaño [1]

[1] Departamento de Física, Universidad de Extremadura, 06071, Badajoz, Spain
[2] Instituto de Computación Científica Avanzada (ICCAEx), Universidad de Extremadura, 06071, Badajoz, Spain
[3] Department of Physical, Chemical and Natural Systems, Pablo de Olavide University, 41013, Sevilla, Spain
* Correspondence: fvega@eaphysics.xyz (F. V. R.)

Abstract: We study an air-fluidized granular monolayer, composed in this case of plastic spheres, which roll on a metallic grid. The air current is adjusted so that the spheres never loose contact with the grid, so that the dynamics may be regarded as pseudo two-dimensional (or two-dimensional, if the effects of sphere rolling are not taken into account). We find two surprising continuous transitions, both of them displaying two coexisting phases. Moreover, in all cases, we found the coexisting phases display strong energy non-equipartition. In the first transition, at weak fludization, a glassy phase coexists with a disordered fluid-like phase. In the second transition, a hexagonal crystal coexists with the fluid phase. We analyze, for these two-phase systems, the specific diffusive properties of each phase, as well as the velocity correlations. Surprisingly, we find a glass phase at very low packing fraction and for a wide range of granular temperatures. Both phases are characterized also by a strong anti-correlated velocities upon collision. Thus, the dynamics observed for this quasi two-dimensional system unveils phase transitions with peculiar properties, very different from the predicted behavior in well know theories for their equilibrium counterparts.

Keywords: phase transition; diffusion; granular matter

1. Introduction

The dynamics of granular matter has been an emerging field for several decades now [1,2]. This is partly due to the many industrial and engineering applications that this kind of materials has [3]; and partly due the fact that, granular set-ups can be used as prototype non-equilibrium systems for experiments [4] and also, from a theoretical viewpoint, they allow for the deployment of the theory of non-equilibrium statistical mechanics [5], fluid mechanics [6] and materials science [7,8]. Moreover advances on granular dynamics theory have clearly put in evidence that, both at mesoscopic and macroscopic level, the dynamics of granular matter has analogous features to that of molecular matter but at the same time presents a much more complex behavior [6]. So, granular dynamics can be regarded, from the theoretical point of view, as an extension or generalization of the dynamics of molecular matter [5,9].

For instance, stratification [3], phase transitions [10–12], ordering [4], pattern formation , segregation [13], mixing [11], fluid convection [14], hydrodynamic instabilities [15], turbulence [16,17], etc. are all phenomena that are known to be present in granular matter in significantly more varied forms and behaviors. For instance, just out of illustration, the set of steady base flows that can be observed in a plane Fourier/Couette configuration (a fluid confined within two infinite parallel walls) includes those that are present in molecular gases plus new steady flows, that are specific of granular fluids [6]. In particular, the Fourier configuration (two static parallel walls) for a molecular gas yields steady flows with constant heat flux; these constant heat flux states are however possible in a granular gas if the confining parallel walls are moving (Couette configuration) [18].

 doi:10.20944/preprints202209.0329.v1

In this work, we focus instead in the phase transitions, and order/disorder phenomenology in a two-dimensional system. As it is well known, an equilibrium fluid in two-dimensions (2D) crystallizes to a hexagonal phase (the hexatic phase) via a continuous transition that is mediated by a phase that is specific of two dimensions. This process is well described by the KTHNY scenario (from their main authors Kösterlitz, Thouless, Halperin, Nelson, Young; see their independent works [19–22]). The new hexatic phase appears exclusively in 2D and is characterized by having quasi-long-ranged translational correlations (with power-law decay) and short-ranged translational correlations (with exponential decay). This liquid-hexatic-crystal scenario has also been observed in a monolayer of vertically vibrated macroscopic spheres [23,24] and in 2D particle simulations of system of active particles [25]. In both cases, however, important departures with respect to the equilibrium phase transition are reported. In effect, the KTHNY scenario appears in both granular and active matter only as a special case within a more complex framework of different combinations of continuous and discontinuous transitions.

Furthermore, it has been reported recently that in a configuration of ping-pong balls rolling over a flat surface the KTHNY is, apparently, absent [26–29]; i.e., no hexatic phase could be detected. Instead, two consecutive phase transitions were detected, both with two coexisting phases. In the first one, at low granular temperature, a glass is observed in coexistence with the arrest phase (with this term, we refer to particles that at very low energy input are still static due to friction [4,30]). The second phase coexistence occurs at higher packing fraction, in which we can observe in certain ranges of driving intensity a coexistence between a liquid and a hexagonal crystal [28].

In summary, the phase behavior of a monolayer of rolling spheres seems to suggest that dynamics of each of the observed phases would have very peculiar properties with respect to the 2D (either equilibrium or non-equilibrium) analogs discussed above. Thus, a detailed analysis of the dynamics of the phases of rolling spheres is needed. Moreover, in order to complete the description of non-equilibrium 2D phase transitions, whose relevance we have discussed above, this analysis should be undertaken for each (coexisting) phase separately.

Therefore, we will study in this work the specific features and properties of the dynamics of each of these two coexisting pair of phases. We will show that strong energy non-equipartition occurs between the coexisting phases in all cases. We will also focus specifically on the diffusive properties and velocity autocorrelations of each of the observed phases. We show that the glass and the crystal phases are clearly subdiffusive. Surprisingly, the liquid phase can display either normal diffusion or weakly subdiffusive or superdiffusive behavior. As we will see, these transitions in the diffusive behavior of the system occur in a continuous way. Furthermore, in the glassy phase, particle velocities are strongly anticorrelated at early times, whereas the crystal anticorrelations are weak.

The paper is structured as follows: Section 2 is devoted to the description of the experimental set-up and methods, and also to a qualitative description of the observed phase behavior. In Section 3, the results for particle diffusion and velocity correlations of each of the observed phases are analyzed separately and in detail. Finally, in Section 4 the results and final conclusions are discussed.

2. Description of the experiments

2.1. Setup

The experimental configuration we use in this work was designed in our lab. It consists of an air-table set-up [31]. In our case, it is composed by two essential parts: a) the driving unit, that produces a stable quasi-laminar air upflow, and that consists of a high power fan (SODECA HCT-71-6T); and b) the arena, which consists of a flat metallic plate with a hexagonal lattice of perforated circular holes (of 3 mm diameter) is surrounded by circular walls (PLA plastic) of 4.5 cm height. The metallic plate is carefully levelled to be horizontal (so that gravity does not enter into the dynamics if restrained within the plate). Both parts are connected by a pair of perpendicular channels that conduct the air released

 doi:10.20944/preprints202209.0329.v1

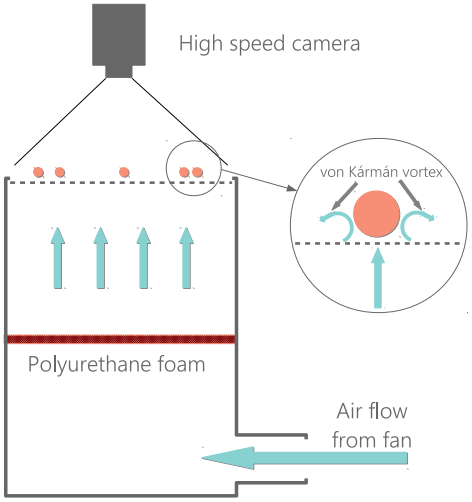

Figure 1. Sketch of the experimental set up.

from the fan upwards to the metallic grid. See Figure 1 for a schematic representation of this configuration. The metallic grid has a square-shaped (80×80 cm^2) but a (circle-shaped) plastic wall is put inside it, centered, so that the particles are enclosed within this circular region of radius $R = 36.25$ cm.

In the middle of the conducting channels there is a foam that homogenizes the upflow, which impinges a set of spherical particles (ping pong balls) disposed over the metallic grid. The spherical particles are all identical, having a diameter of $\sigma = 4$ cm and a mass density $\rho = 0.08$ g cm^{-3} (ABS plastic material). The ping-pong ball configuration is inspired in a previous work by Ohja et al., where the equation of movement of a Brownian particle, consisting on a ping-pong ball in an air table, was solved [32]. Fan power is carefully adjusted so that the particles never loose physical contact with the plate. So, within the appropriate ranges of fan power, air upflow past the spheres produces turbulent vortexes [33] that yield stochastic horizontal movement to the spheres and thus the particle dynamics (if sphere rolling is excluded) is strictly two-dimensional. As fan power is increased, the system passes through a series of different physical configurations which are accessed through phase transitions. We have observed phase coexistence during these transitions, for experiments in a range of values of particle density. We characterize particle density by means of the packing fraction, that here is defined as $\phi \equiv N\sigma^2/R^2$, where N is the number of particles present in the system.

Everything is recorded by means of a high-speed camera (Phantom VEO 410L) at 250 fps. Experiments movies are processed by a particle tracking code that we developed specifically for this configuration. This code is composed by a series of OpenCV [34] and TrackPy [35] functions, which allow to obtain all particle positions over the acquired images and tag each particle so that it will be tracked through the entire movie. Experiments are 100 s long, much higher than the typical transitory time towards the steady state. In this way, a set of $\approx 2 \times 10^4$ steady state statistical replica (corresponding to recorded frames after the transient) are available to process. From these data sets (please refer to the Data Statement at the end of this document), a statistically meaningful description of the magnitudes and configurations here described for each experiment is obtained.

2.2. Phase behavior

Figure 2 presents a series of movie snapshots displaying the different phase states that we have detected in our experiments, for two different packing fraction values. For each packing fraction, snapshots are placed in ascending order of fan power. At the lowest fan power ($\phi = 0.18$, several particles are still static, since the turbulent vortexes intensity is

 doi:10.20944/preprints202209.0329.v1

not strong enough so as to overcome static friction. We denote this static phase as *arrest* phase, due to its static nature. (Eventually, the arrest phase can develop a quasi-static ordered state that has been called traditionally *collapse* phase in analogous configurations [4]). At sufficiently high air current intensity, the vortexes become strong enough so that all particles undergo stochastic movement. However, we can observe caging effects for these particles. Here, we have detected coexistence between the arrest phase and a glassy phase for the caged moving particles (Figure 2 a). The arrest phase eventually disappears, then giving rise to glass-liquid phase coexistence (Figure 2 b). At higher density ($\phi = 0.55$, we observe consecutively: liquid phase (Figure 2 c), crystal coexistence (Figure 2 d), and crystal-liquid phase (Figure 2 e). At this point, if fan power is still increased, a shrink of the crystal (that *melts*), with the crystal completely disappearing at high enough air current intensity. This last stage is not represented since they look much like the snapshots in Figure 2 (c),(d). In any case, grasping the phase configuration out of these snapshots is not straightforward and for this reason we analyze in more detail the particle trajectory structure in the next section.

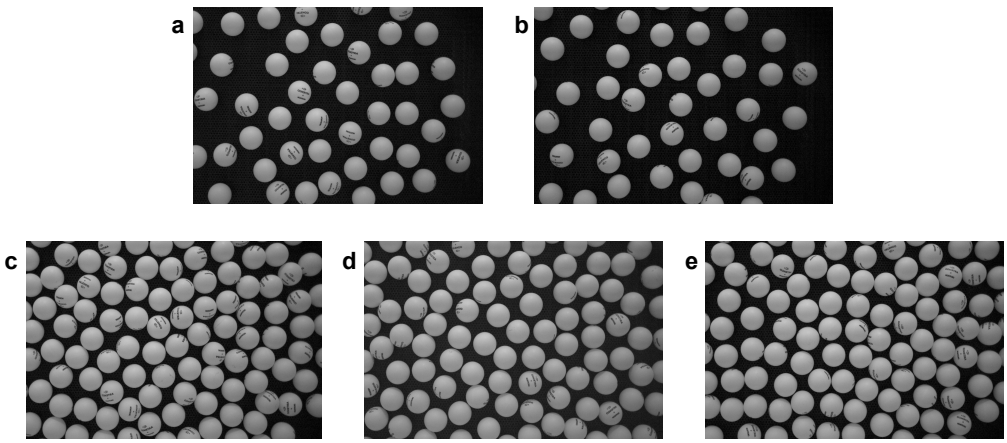

Figure 2. Snapshots of the different phase configurations observed in experiments. Packing fraction is $\phi = 0.18$ for (a)-(b) and $\phi = 0.55$ for (c)-(e). Granular temperatures are, in order: $T/m = [0.16,\ 0.74,\ 0.38,\ 0.47,\ 0.70]\ \sigma^2 s^{-2}$ for the configurations (same order): glass-arrest phase, glass-liquid, liquid, crystal, crystal-lquid.

3. Results

3.1. Trajectories and granular temperature field

In order to analyze in more detail the dynamic properties (except for the static arrest phase), we compute separately the trajectory shape, temperature field, diffusion coefficient, and velocity autocorrelations of each of the observed phases.

So, Figure 3 shows particle trajectories (left column) and granular temperature fields for a representative set of experiments. The experiments correspond to two different densities (low and high), with each subset in ascending order of upflow current, so that we can see the phases that consecutively appear as more energy is input into the system. Figure 3 (a) shows two qualitatively different types of arrangements of particle trajectories phases: a disordered lattice of particle trajectories (moving particles that remain close to a disordered set of fixed points), and a disordered lattice of static particles (arrest phase). In effect, the former set of trajectories can be identified as a glassy phase since, although particles undergo continuous stochastic movement, caging effects are predominant [36,37] and a disordered but permanent particle trajectory structure (lattice) can be observed. To

 doi:10.20944/preprints202209.0329.v1

our knowledge, it is not very common to find glass transitions at such low densities. With respect to the latter, it is apparent that particles remain static during the complete 100 s experiment. From this qualitative difference between these two phases a strong energy non-equipartition emerges. In effect, as we can see in Figure 3 (b), the region corresponding to the arrest phase has vanishing granular temperature T whereas for the glassy phase T is clearly non-null. Note that, contrary to what has been observed in thin layers, the static phase does not necessarily appear as a hexagonally ordered collapse phase, as in a vertically vibrated monolayer of spheres. This peculiar arrest phase, that is present also in a vibrated granular monolayer [30], disappears here gradually as the upflow current is increased, to a point where we can observe two-phase coexistence between glass-like and liquid-like phases, as in Figure 3 (c), where the liquid phase is observed in the region where all trajectories mix and cross each other during the experiment, in contrast with the disordered pattern of localized trajectories that is visible in the upper left corner. As we can see in Figure 3 (d), energy non-equipartition is strong here again, with the glass phase being noticeably cooler. At higher density (packing fraction $\phi = 0.55$), we observe, consecutively, a monophase liquid-like system (Figure 3 e-f); a hexagonal crystal phase (Figure 3 g-h); and a two-phase system, with a liquid coexisting with a hexagonal lattice (Figure 3 i-j). Notice also that non-equipartition is also present in the case of the liquid-crystal two phase system, with the crystal colder than the liquid (Figure 3 h).

Preprints (www.preprints.org) | NOT PEER-REVIEWED | Posted: 22 September 2022 doi:10.20944/preprints202209.0329.v1

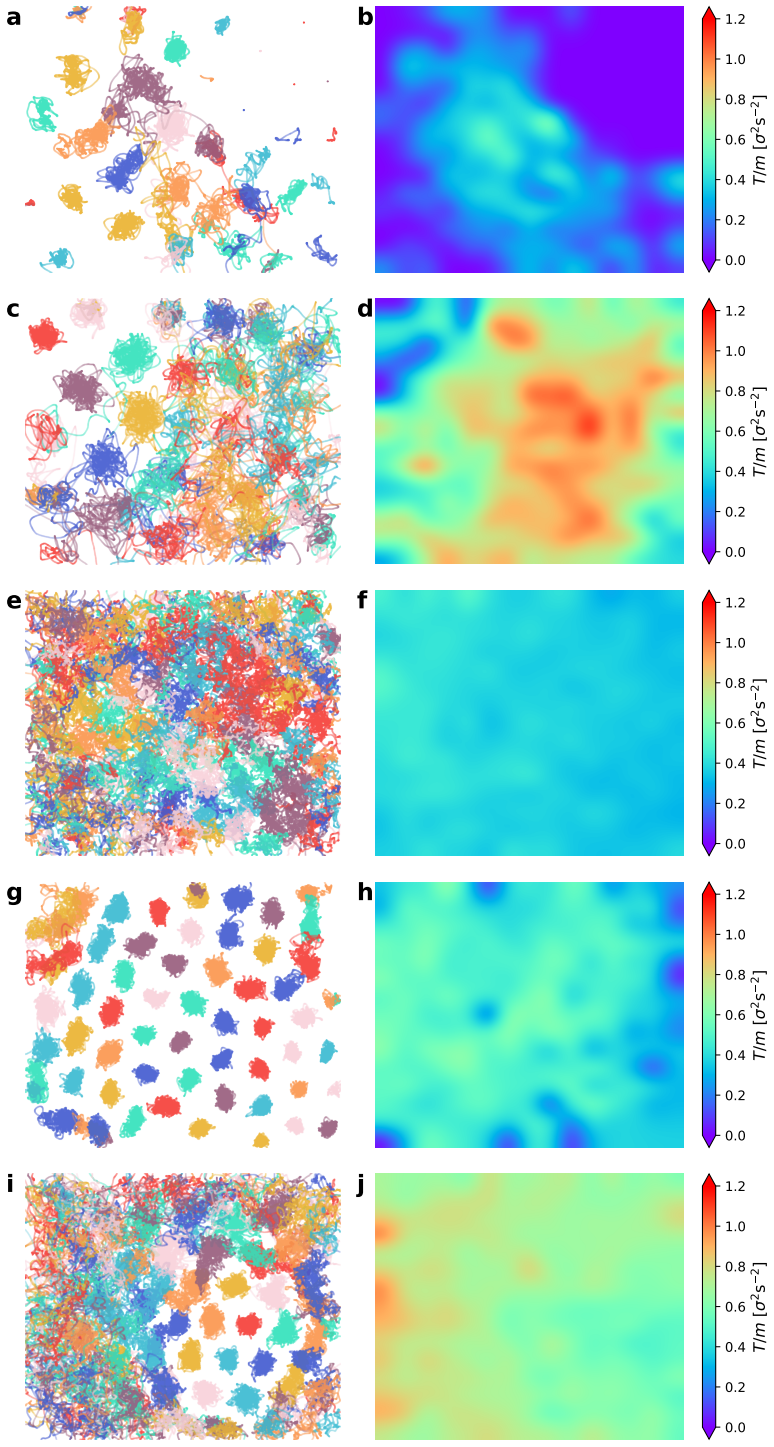

Figure 3. Phase behavior of our system, in a central region of interest. Left column represents particle trajectories; right column shows the corresponding granular temperature 2D fields (T). Packing fraction is $\phi = 0.18$ for (a)-(d) and $\phi = 0.55$ for (e)-(j). Meanwhile, granular temperatures for each pair of panels are, respectively: $T/m = [0.16,\ 0.74,\ 0.38,\ 0.47,\ 0.70]\ \sigma^2 s^{-2}$. In (a)-(b) we can see phase coexistence between a glassy phase and the arrest phase at low density. In (c)-(d), low density but higher T, there is glass and liquid phase coexistence. (e)-(f) shows that the system is completely disordered (there is only a liquid phase), state that can be observed at intermediate temperatures for all densities. At higher densities, if the liquid is further heated (air upflow is increased), a cooler crystallite develops in coexistence with the liquid, as in (g)-(h). At stronger driving, the liquid tends to disappear and the crystal occupies the whole system.

Preprints (www.preprints.org) | NOT PEER-REVIEWED | Posted: 22 September 2022 doi:10.20944/preprints202209.0329.v1

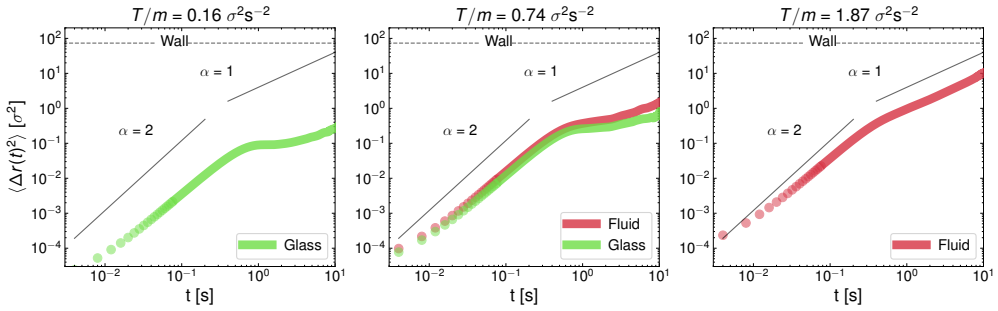

Figure 4. Mean squared displacement for three representative experiments of $\phi = 0.18$, the central panel corresponds to the case presented in Figure 3(c)-(d).

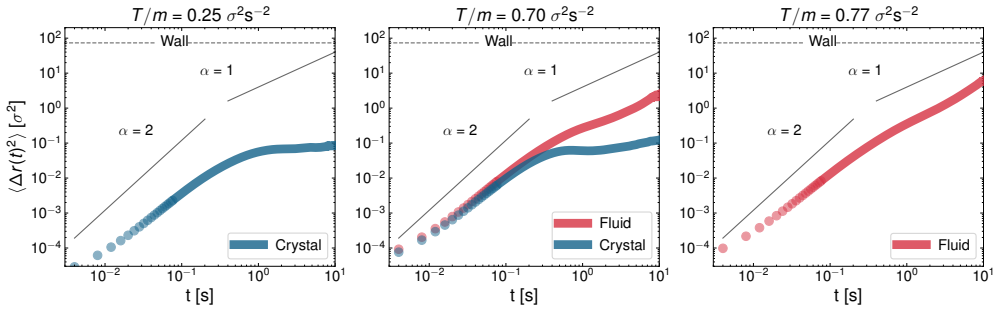

Figure 5. Mean squared displacement for three representative experiments of $\phi = 0.55$. The central panel corresponds to the case presented in Figure 3(i)-(j).

Overall, the fact that non-equipartition is noticeably present in all two-phase system configuration denotes that each phase has its own peculiar dynamics. In particular, this can be an indication that the diffusion process in each phase might have different scales and behavior [38]. Specially because the structure of Brownian trajectories in each phase is very different, as trajectories in the left column of Figure 3 show. For this reason, by identifying first which trajectories belong to each phase in all experiments, we have computed the diffusion coefficient for each phase. We have done so by tracking the mean squared displacement (MSD) for each phase, Figures 4, 5 show the evolution of ensemble mean squared displacements, that in 2D can be defined as [39]

$$\langle \Delta r(t)^2 \rangle \equiv \langle \Delta x(t)^2 + \Delta y(t)^2 \rangle, \tag{1}$$

where $\Delta x(t)^2 \equiv (1/\mathcal{N}(t)) \sum_{\{t_0\}} [x(t+t_0) - x(t_0)]^2$ (and analogously for $\Delta y(t)^2$). For each lag time under steady state conditions, the squared displacements $\Delta x(t)^2, \Delta y(t)^2$ can be obtained from averages on the $\mathcal{N}(t)$ available initial times t_0. As a guide to the eye, the ballistic ($\alpha = 2$) and normal ($\alpha = 1$) diffusion values were indicated inside each panel in Figures 4, 5.

More specifically, in Figure 4 we can see the following cases: observed; glass (a), glass-liquid (b), liquid (c); whereas in Figure 5 we can see the cases: only crystal (a), crystal-liquid (b) and only liquid(c). It is very apparent that the behavior of the MSD for each phase is very different. In particular, the monophase glassy configuration (Figure 4 a) presents an MSD with a local maximum at the end of the ballistic regime, after which it presents a characteristic curvature in the diffusive part of the curve, which is besides strongly subdiffusive. The MSD behaviour of the glass-like phase is thus characterized by a short plateau in the MSD followed by an increase (when particles escape the current "caging" area and move to a new location. At higher T, in Figure 4 (b), we can see the glass-liquid coexistence. In this case, the emerging liquid phase is still weakly subdiffusive (although with a clearly faster MSD, if compared to the companion glass). In Figure 4 (c), the system with only liquid phase shows already a normal diffusion scenario. By contrast, Figure 5 (a) shows a single crystal configuration, with the diffusive part of the MSD close to stagnation

Preprints (www.preprints.org) | NOT PEER-REVIEWED | Posted: 22 September 2022 doi:10.20944/preprints202209.0329.v1

(zero time growth of the MSD); i.e., the dynamics is very strongly subdiffusive. In the case of crystal-liquid coexistence, Figure 5 (b), the less disordered phase (glass) clearly undergoes subdiffusion, whereas the liquid has normal diffusion. Normal diffusion can also be seen in Figure 5 (c), where the single liquid phase is recovered. An important and surprising result is the observation of glassy transitions with clear caging processes at low densities, when in general these processes are observed (to the best of our knowledge) in dense granular fluids [40]. This result may be the outcome of an effective potential developed by the interaction between the spherical balls through the intermediate air flow.

3.2. Diffusion coefficient

Thus, from the results in Figures 4, 5, we may conclude that the evolution of the MSD for each phase is qualitatively very different. For this reason, we compute the diffusion coefficient separately for each phase, according to the relation [38]

$$\langle \Delta r(t)^2 \rangle = (4D)t^{\alpha}, \tag{2}$$

where α is the diffusive exponent, previously obtained from a linear fit in the diffusive part (after ballistic regime) of the MSD in curves of the type displayed in Figure 4. This diffusive exponent is, as it is known, $\alpha = 2$ for the ballistic regime and $\alpha = 1$ for the diffusive regime, if diffusion is *normal* (and $\alpha < 1$ for subdiffusion, $2 > \alpha > 1$ for superdiffusion [38]).

Therefore, we represent in two figures our measurements of the diffusion coefficient. In Figure 6, D is represented vs. packing fraction, for a series of experiments in different ranges of T: $T/m < 0.6\ \sigma^2/s^2$; $0.6\ \sigma^2/s^2 < T/m < 0.8\ \sigma^2/s^2$; $0.8\ \sigma^2/s^2 < T/m < 1.2\ \sigma^2/s^2$ and $T/m > 1.2\ \sigma^2/s^2$, whereas in Figure 7, we plot D vs. T for three representative packing fraction values ($\phi = 0.18; 0.46; 0.55$). Figure 6 highlights the diffusive stages of the different phase configurations, including those with phase coexistence (the coexisting phases are here joined with dashed vertical lines). As we can see, at $T/m < 0.6\ \sigma^2/s^2$ (top left panel), the diffusion coefficient tends to decrease for increasing ϕ in general. Moreover, only glass or liquid phases are visible at very low T, with the liquid coexisting with the glass at low packing fractions whereas at intermediate packing fractions we find crystal-liquid coexistence and at larger ϕ only the crystal is detected, in this case with the lowest D values. At higher intermediate temperatures (at $0.6\ \sigma^2/s^2 < T/m < 0.8\ \sigma^2/s^2$, in top right panel; and at $0.8\ \sigma^2/s^2 < T/m < 1.2\ \sigma^2/s^2$, bottom left) we can see the glass-liquid at low density again the effects of larger T cause the withdrawal of the crystal-liquid coexistence at intermediate ϕ, leaving the liquid (red symbols) alone. Again, at higher ϕ, crystal-liquid and crystal are detected. Finally, in the largest range of values of T, it is apparent that only the liquid is observed (except for a configuration with the densest system we used) and that in this regime the diffusion coefficient is nearly constant with respect to packing fraction, except for a steep decay at large ϕ (where the only two cases of coexistence with a crystal are here observed). It is also interesting to note that an extrapolation of the curve averaged by the crystalline states extends to the low-density glass transition zones. In summary, D tends to decrease for denser systems, except at very high T, where it tends to keep approximately constant.

Now, in Figure 7, which represents D vs. T, summarizes well the quantitative differences in the diffusion coefficient for the three phases (glass, liquid, crystal), together with the ranges of coexistence of glass and crystal with the liquid phase. Overall, liquid predominates at low and moderate density (left and center panels), whereas glass and crystal predominate at very low and high density respectively. It can also be observed that both glass and crystal are less diffusive than the liquid, as it was to be expected, with the crystal having the lowest values, systematically, of the diffusion coefficient.

As we mentioned before, previously to computing the diffusion coefficient we determine the diffusive exponent α as defined by eq. (2), and whose value defines if the system is under super-diffusion ($\alpha > 1$), sub-diffusion ($\alpha < 1$) or normal diffusion ($\alpha = 1$) [38,39]. So, we plot in Figure 8 the measurement of α for all the performed experiments altogether. They are represented as a function system granular temperature T for all the

Preprints (www.preprints.org) | NOT PEER-REVIEWED | Posted: 22 September 2022 doi:10.20944/preprints202209.0329.v1

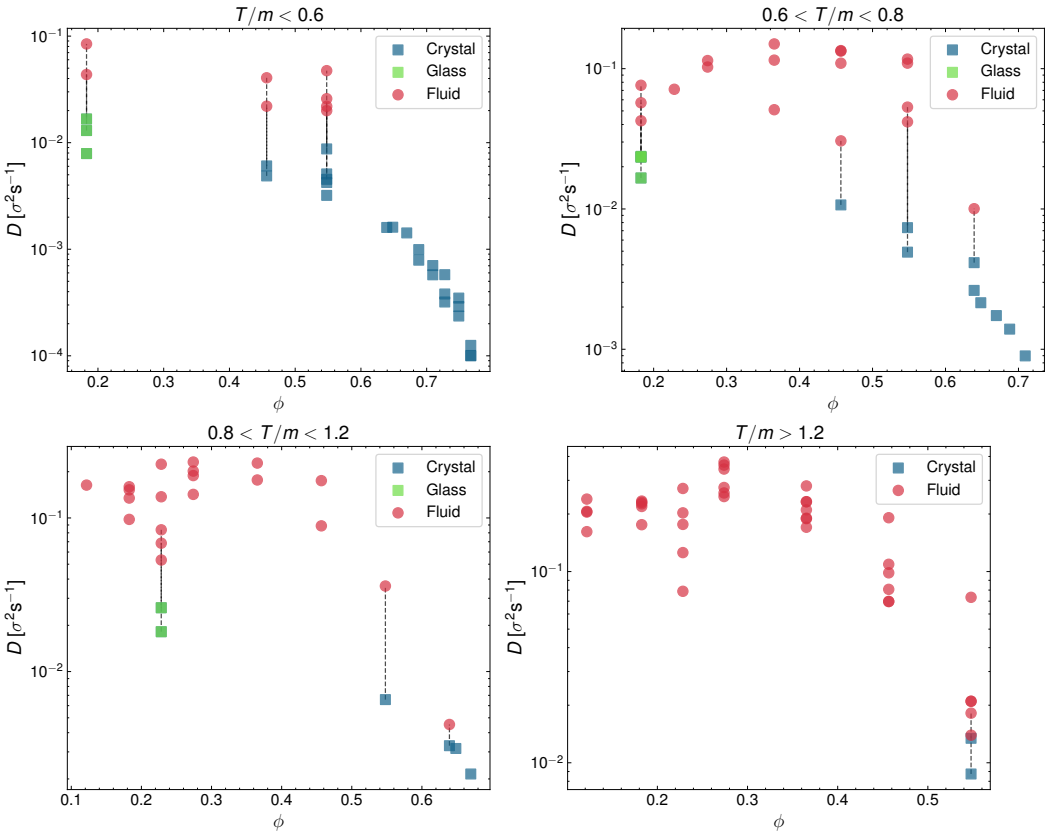

Figure 6. Diffusion coefficient D vs. packing fraction ϕ divided in four panels by the overall granular temperature of each experiment.

particle densities combined (here, represented in the form of packing fraction ϕ). Red points signal the liquid phase diffusive exponents, green stands for the glass phase and blue for the crystal. As we can see, diffusion is weakest in the crystal phase, with very low values of α. The glass phases is also very subdiffusive, but in general with stronger diffusion as compared to the crystal. The liquid however can be either weakly sub-diffusive or weakly superdiffusive, oscillating around the normal diffusion value for all experiments, except in the range of very low T, where the distinction between glass and liquid is not entirely clear.

3.3. Velocity autocorrelations

We also represented the velocity autocorrelation function, computing its trend for glass, liquid and crystal. Velocity autocorrelations provide information on the dynamics of particle collision, in particular on the statistical relation between pre-collisional and post-collisional velocities. We define the velocity autocorrelation function at lag time τ as usual [11]

$$A_{\mathbf{v}}(\tau) = \frac{\langle \mathbf{v}(t) \cdot \mathbf{v}(t+\tau) \rangle}{\langle \mathbf{v}(t) \cdot \mathbf{v}(t) \rangle}, \tag{3}$$

where here $\langle \dots \rangle$ stands for ensemble averaging over all steady states at initial times t_0. Figure 9 represents velocity correlations $A_{\mathbf{v}}(\tau)$ in the glass-liquid transition and Figure 10 represents $A_{\mathbf{v}}(\tau)$ for the crystal-liquid transition. It is to be noted that particles in the glass phase (left panel in Figure 9) show strong velocity anticorrelations at early times ($A_{\mathbf{v}}(\tau < 1) < 0$) and that these anticorrelations are transmitted to the coexisting liquid (center panel of Figure 9). Surprisingly as well, the depth of the anticorrelation well is increased in the glass-liquid two-phase system, with respect to the pure glass (left panel). Furthermore, the liquid remains anticorrelated at $\tau < 1$ even when the glass has disappeared at high T. By contrast, the pure liquid phase does not display autocorrelations

Preprints (www.preprints.org) | NOT PEER-REVIEWED | Posted: 22 September 2022 doi:10.20944/preprints202209.0329.v1

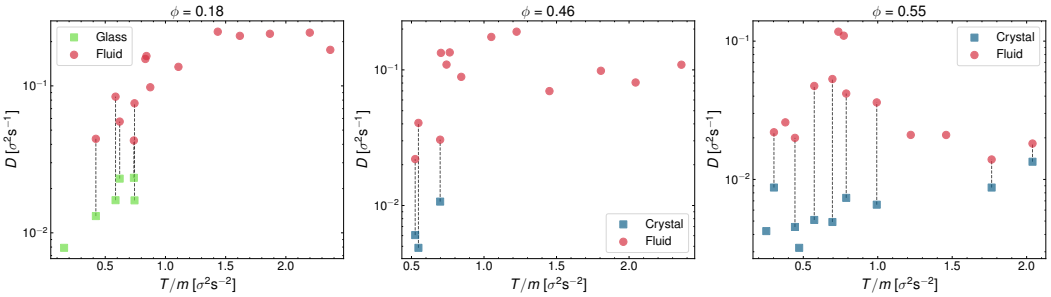

Figure 7. Average diffusion coefficients represented against granular temperature for three different packing fractions. Each point corresponds to an experiment; where coexistence is visible, we have split D into two different points, for the fluid (red) and crystal/glass phase (blue/green).

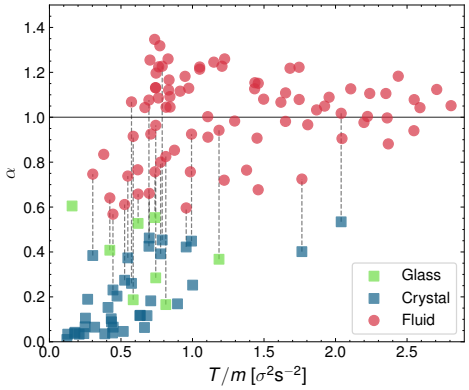

Figure 8. Diffusive exponent represented against granular temperature for all experiments. It has been calculated by averaging the logarithmic slope of the MSD in the [3-6] s range. Each point corresponds to an experiment; where coexistence is visible, we have split D into two different points, for the fluid (red) and crystal/glass phase (blue/green).

in the crystal-liquid transition (right panel in Figure 10), as well as an increase in the time required for the autocorrelation function to cancel for the first time. However, there are weaker anticorrelations in the pure crystal (left panel in Figure 10) and crystal-liquid two-phase state, and a very short time for the first cancellation of the autocorrelation function, typical of the crystal phase. Let us remark here that the right panels in Figures 9, 10 combined reveal that the liquid phase has a variety of internal behaviors. This variety of behavior is closely related to the occurrence of the glass transition at low densities, because as mentioned before, at low densities there is a repulsive interaction between the particles mediated by the upward air flow (as if they had a soft core with a diameter greater than that of the balls), and when the density is increased, this effective potential does not prevent the direct collision between the spherical balls.

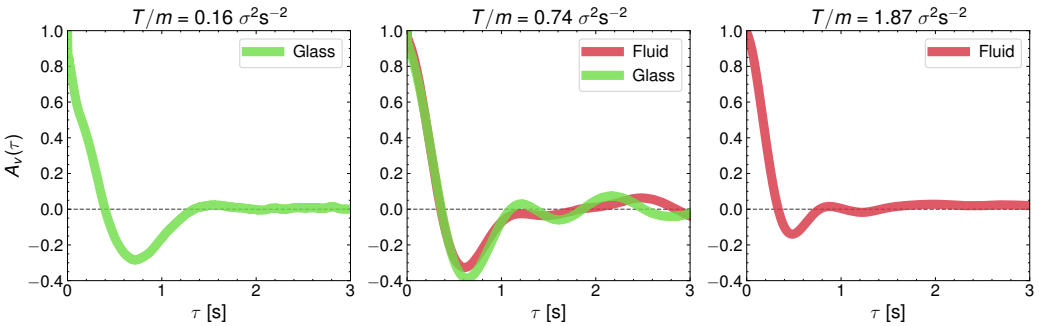

Figure 9. Normalized velocity autocorrelation for three different temperatures at $\phi = 0.18$. They correspond to the cases presented for the MSD in Figure 4.

Preprints (www.preprints.org) | NOT PEER-REVIEWED | Posted: 22 September 2022 doi:10.20944/preprints202209.0329.v1

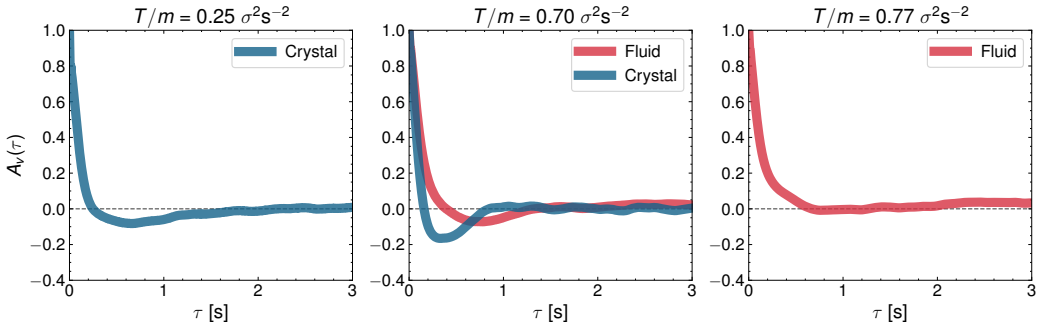

Figure 10. Normalized velocity autocorrelation for three representative experiments of $\phi = 0.55$. They correspond to the cases presented for the MSD in Figure 5.

4. Discussion

We have studied the nearly-2D dynamics of a system of rolling (inelastic) spheres. The dynamics of the set of spheres is activated by means of the turbulent vortexes that originate out of an air upflow past the spheres. As we have seen, the phase behavior of the system is very complex, and we have been able to detect an arrest phase (particles that remain still or static for low energy input), a glass phase (disordered lattice of Brownian particles with sporadic jumps to other lattice positions), a liquid (completely disordered phase) and a hexagonal crystal. In particular, the glass phase appears at very low densities, which to our knowledge is a very rare situation [37]. Moreover, the glass and the hexagonal crystal can coexist with the liquid. Additionally, the glass can also coexist with the arrest phase, at low air current (dynamics in the process of activation). In fact, the dynamics of the system is so complex that we have been able to detect important qualitative differences in the behavior of a single phase. For instance, as we mentioned above, the velocities of particles in the liquid phase can be either strongly anticorrelated at early times or not anticorrelated at all, depending on the configuration of the system. As another example, the crystal can display vanishing diffusive exponent (and in any case, the crystal is always very subdiffusive, see Figure 8).

In general, the diffusive properties of the observed phases are rather different. Both the glass and the crystal are always subdiffusive, and present anticorrelated velocities. By contrast, the liquid presents always nearly normal diffusion (departures from normal diffusion can be attributed here either to measurement error or to limitations of our set-up). Measurement of the granular temperature field confirms that in all cases of phase coexistence there is a significant energy non-equipartition. This enhances the idea that these transitions are occurring in states very far from equilibrium. It may be that because of this (that our experimental configurations seem to be very far away from equilibrium) the phase transition scenario here described completely differs from the KTHNY scenario described for 2D equilibrium systems [41] and also, under certain conditions, in non-equilibrium systems such as a vibrated granular monolayer [23,24] and 2D active brownian disks [25]. Here, however, this KTHNY scenario is absent and the hexatic phase has not been observed. Furthermore, all transitions we observed in this work occur through phase coexistence, contrary to the scenario of liquid-hexatic-crystal continuous phase transition described in the KTHNY theory. Therefore, our results differ fundamentally in this aspect from previous results in both equilibrium and non-equilibrium systems (where the hexatic phase has always been observed, at least, under certain conditions). It remains for future work to study in more detail the structure of this intriguing phase behavior.

Author Contributions: J.F. G.-S. and M. A. L.-C. performed all the experiments. M. A. L.-C. and F. V. R. developed the particle tracking and processing codes. M.A. L-.C. prepared all figures. All authors participated in the formal analysis of the experimental data. A. R.-R. and F. V. R. reviewed and edited the manuscript. Design of the experiment, conceptualization, original draft preparation, and supervision was performed by F. V. R. All authors have read and agreed to the published version of the manuscript."

Funding: We acknowledge funding from the Government of Spain through Agencia Estatal de Investigación (AEI) project No. PID2020-116567GB-C22). A.R.-R. also acknowledges financial support from Consejería de Transformación Económica, Industria, Conocimiento y Universidades de la Junta de Andalucía/FEDER for funding through project P20-00816 and FSE through post-doctoral grant no. DC00316 (PAIDI 2020). F. V. R. is supported by the Junta de Extremadura grant No. GR21091, partially funded by the ERDF. The APC was funded by the MDPI editorial.

Data Availability Statement: Experimental data tables and trajectories are available in a public repository, at:
`https://doi.org/10.5281/zenodo.7097642`.

Acknowledgments: The authors are indebted to the Taller de Mecánica de la Escuela de Ingenierías Industriales for construction of the air table.

Conflicts of Interest: The authors declare no conflict of interest.

References

1. Jaeger, H.M.; Nagel, S.; Behringer, R. The physics of granular materials. *Physics Today* **1996**, *49*, 32.
2. de Gennes, P.G. Granular matter: a tentative view. *Rev. Mod. Phys.* **1999**, *71*, S374–S382.
3. Aranson, I.S.; Tsimring, L.S. Patterns and collective behavior in granular media: Theoretical concepts. *Rev. Mod. Phys.* **2006**, *78*, 641–692. https://doi.org/10.1103/RevModPhys.78.641.
4. Olafsen, J.S.; Urbach, J.S. Clustering, order and collapse in a driven granular monolayer. *Phys. Rev. Lett* **1998**, *81*, 4369–4372.
5. Goldhirsch, I. Rapid Granular Flows. *Annu. Rev. Fluid Mech.* **2003**, *35*, 267–293.
6. Vega Reyes, F.; Urbach, J.S. Steady base states for Navier-Stokes granular hydrolodynamics with boundary heating and shear. *J. Fluid Mech.* **2009**, *636*, 279.
7. Gantzounis, G.; Yang, J.; Kevrekidis, P.G.; Daraio, C. Granular acoustic switches and logic elements. *Nat. Commun.* **2014**, *5*, 5311. https://doi.org/10.1038/ncomms6311.
8. González-Saavedra, J.F.; Rodríguez-Rivas, Á.; López-Castaño, M.A.; Vega Reyes, F. Acoustic Resonances in a Confined Set of Disks. In Proceedings of the Traffic and Granular Flow 2019; Zuriguel, I.; Garcimartin, A.; Cruz, R., Eds.; Springer International Publishing: Cham, 2020; pp. 349–355.
9. Mujica, N.; Soto, R. Dynamics of Noncohesive Confined Granular Media. In Proceedings of the Recent Advances in Fluid Dynamics with Environmental Applications; Klapp, J.; Sigalotti, L.D.G.; Medina, A.; López, A.; Ruiz-Chavarría, G., Eds.; Springer International Publishing: Cham, 2016; pp. 445–463.
10. Prevost, A.; Melby, P.; Egolf, D.A.; Urbach, J.S. Nonequilibrium two-phase coexistence in a confined granular layer. *Phys. Rev. E* **2004**, *70*, 050301. https://doi.org/10.1103/PhysRevE.70.050301.
11. Melby, P.; Vega Reyes, F.; Prevost, A.; Robertson, R.; Kumar, P.; Egolf, D.A.; Urbach, J.S. The dynamics of thin vibrated granular layers. *J. Phys.: Condens. Matter* **2005**, *17*, S2369.
12. Vega Reyes, F.; Urbach, J.S. Effect of inelasticity on the phase transitions of a thin vibrated granular layer. *Phys. Rev. E* **2008**, *78*, 051301. https://doi.org/10.1103/PhysRevE.78.051301.
13. Hill, K.M.; Khakhar, D.V.; Gilchrist, J.F.; McCarthy, J.J.; Ottino, J.M. Segregation-driven organization in chaotic granular flows. *Proceedings of the National Academy of Sciences* **1999**, *96*, 11701–11706, [https://www.pnas.org/doi/pdf/10.1073/pnas.96.21.11701]. https://doi.org/10.1073/pnas.96.21.11701.
14. Rodríguez-Rivas, A.; López-Castaño, M.A.; Vega Reyes, F. Zero-gravity thermal convection in granular gases. *Phys. Rev. E* **2020**, *102*, 010901. https://doi.org/10.1103/PhysRevE.102.010901.
15. Eshuis, P.; van der Weele, K.; van der Meer, D.; Bos, R.; Lohse, D. Phase diagram of vertically shaken granular matter. *Phys. Fluids* **2007**, *19*, 123301.
16. Isobe, M. Statistical law of turbulence in granular gas. *J. Phys. Conf. Ser.* **2012**, *402*, 012041.
17. Isobe, M. Velocity statistics in two-dimensional granular turbulence. *Phys. Rev. E* **2003**, *68*, 040301(R).
18. Vega Reyes, F.; Santos, A.; Garzó, V. Non-Newtonian Granular Hydrodynamics. What Do the Inelastic Simple Shear Flow and the Elastic Fourier Flow Have in Common? *Phys. Rev. Lett.* **2010**, *104*, 028001. https://doi.org/10.1103/PhysRevLett.104.028001.
19. Kosterlitz, J.M.; Thouless, D.J. Long range order and metastability in two dimensional solids and superfluids. (Application of dislocation theory). *J. Phys. C* **1972**, *5*, L124–L126.
20. Kosterlitz, J.M.; Thouless, D.J. Ordering, metastability and phase transitions in two-dimensional systems. *J. Phys. C* **1973**, *6*, 1181.
21. Nelson, D.R.; Halperin, B.I. Dislocation mediated melting in two dimensions. *Phys. Rev. B* **1979**, *19*, 2457.
22. Young, A.P. Melting and the vector Coulomb gas in two dimensions. *Phys. Rev. B* **1979**, *19*, 1855.
23. Olafsen, J.S.; Urbach, J.S. Two-Dimensional Melting Far from Equilibrium in a Granular Monolayer. *Phys. Rev. Lett.* **2005**, *95*, 098002.
24. Komatsu, Y.; Tanaka, H. Roles of Energy Dissipation in a Liquid-Solid Transition of Out-of-Equilibrium Systems. *Phys. Rev. X* **2015**, *5*, 031025.

25. Digregorio, P.; Levis, D.; Suma, A.; Cugliandolo, L.F.; Gonnella, G.; Pagonabarraga, I. Full Phase Diagram of Active Brownian Disks: From Melting to Motility-Induced Phase Separation. *Phys. Rev. Lett.* **2018**, *121*, 098003. https://doi.org/10.1103/PhysRevLett.121.098003.
26. Abate, A.R.; Durian, D.J. Partition of energy for air-fluidized grains. *Phys. Rev. E* **2005**, *72*, 031305.
27. López-Castaño, M.A.; González-Saavedra, J.F.; Rodríguez-Rivas, Á.; Vega Reyes, F. Statistical Properties of a Granular Gas Fluidized by Turbulent Air Wakes. In Proceedings of the Traffic and Granular Flow 2019; Zuriguel, I.; Garcimartin, A.; Cruz, R., Eds.; Springer International Publishing: Cham, 2020; pp. 397–403.
28. López-Castaño, M.A.; González-Saavedra, J.F.; Rodríguez-Rivas, A.; Abad, E.; Yuste, S.B.; Vega Reyes, F. Pseudo-two-dimensional dynamics in a system of macroscopic rolling spheres. *Phys. Rev. E* **2021**, *103*, 042903. https://doi.org/10.1103/PhysRevE.103.042903.
29. Koyama, S.; Matsuno, T.; Noguchi, T. Anomalous diffusion in a monolayer of lightweight spheres fluidized in air flow. *Phys. Rev. E* **2021**, *104*, 054901. https://doi.org/10.1103/PhysRevE.104.054901.
30. Néel, B.; Rondini, I.; Turzillo, A.; Mujica, N.; Soto, R. Dynamics of a first-order transition to an absorbing state. *Phys. Rev. E* **2014**, *89*, 042206. https://doi.org/10.1103/PhysRevE.89.042206.
31. Maw, N.; Barber, J.R.; Fawcett, J.N. The Role of Elastic Tangential Compliance in Oblique Impact. *Journal of Lubrication Technology* **1981**, *103*, 74–80, [https://asmedigitalcollection.asme.org/tribology/article-pdf/103/1/74/5796519/74_1.pdf]. https://doi.org/10.1115/1.3251617.
32. Ojha, R.P.; Lemieux, P.A.; Dixon, P.K.; Liu, A.J.; Durian, D.J. Statistical mechanics of a gas-fluidized particle. *Nature* **2004**, *427*, 521.
33. Van Dyke, M. *An album of fluid motion*; The Parabolic Press: Stanford, CA, USA, 1982.
34. OpenCV. `https://opencv.org/`.
35. Allan, D. *et al.*. soft-matter/trackpy: Trackpy v0.4.2, 2019.
36. Desmond, K.W.; Weeks, E.R. Random close packing of disks and spheres in confined geometries. *Physical Review E - Statistical, Nonlinear, and Soft Matter Physics* **2009**, *80*, 1–11, [0903.0864]. https://doi.org/10.1103/PhysRevE.80.051305.
37. Rodríguez-Rivas, A.; Romero-Enrique, J.M.; Rull, L.F. Molecular simulation study of the glass transition in a soft primitive model for ionic liquids. *Mol. Phys.* **2019**, *117*, 3941–3956. https://doi.org/10.1080/00268976.2019.1674935.
38. Metzler, R.; Jeon, J.H.; Cherstvy, A.G.; Barkai, E. Anomalous diffusion models and their properties: non-stationarity, non-ergodicity, and ageing at the centenary of single particle tracking. *Phys. Chem. Chem. Phys.* **2014**, *16*, 24128–24164. https://doi.org/10.1039/C4CP03465A.
39. López-Castaño, M.A.; Vega Reyes, F.; Rodríguez-Rivas, A. Diffusive regimes in a two-dimensional chiral fluid. *Comms. Phys.* **2022**, *to appear*. preprint: arXiv:2202.08920.
40. Kranz, W.T.; M. Sperl, .; Zippelius, A. Glass Transition for Driven Granular Fluids. *Phys. Rev. Lett.* **2010**, *104*.
41. Strandburg, K.J. Two-dimensional melting. *Rev. Mod. Phys.* **1988**, *60*, 161.